

# Inferring genetic fitness from genomic data

Hong-Li Zeng<sup>1,2,\*</sup> and Erik Aurell<sup>3,4,†</sup>

<sup>1</sup>*School of Science, and New Energy Technology Engineering Laboratory of Jiangsu Province, Nanjing University of Posts and Telecommunications, Nanjing 210023, China*

<sup>2</sup>*Nordita, Royal Institute of Technology, and Stockholm University, SE-10691 Stockholm, Sweden*

<sup>3</sup>*KTH – Royal Institute of Technology, AlbaNova University Center, SE-106 91 Stockholm, Sweden*

<sup>4</sup>*Faculty of Physics, Astronomy and Applied Computer Science, Jagiellonian University, 30-348 Kraków, Poland*

(Dated: February 9, 2022)

The genetic composition of a naturally developing population is considered as due to mutation, selection, genetic drift and recombination. Selection is modeled as single-locus terms (additive fitness) and two-loci terms (pairwise epistatic fitness). The problem is posed to infer epistatic fitness from population-wide whole-genome data from a time series of a developing population. We generate such data in silico, and show that in the Quasi-Linkage Equilibrium (QLE) phase of Kimura, Neher and Shraiman, that pertains at high enough recombination rates and low enough mutation rates, epistatic fitness can be quantitatively correctly inferred using inverse Ising/Potts methods.

## I. INTRODUCTION

The last ten years has seen an explosion of interest in results obtained from inferring terms in Ising or Potts models from data [1]. When applied in biological data analysis this approach is known as Direct Coupling Analysis (DCA) and has led to a breakthrough in identifying spatial contacts in proteins from protein sequence data [2–6], which in turn has been used to predict spatial contacts from the sequence data [7–9]. DCA has also been used to identify nucleotide-nucleotide contacts of RNAs [10], multiple-scale protein-protein interactions [11, 12], amino acid-nucleotide interaction in RNA-protein complexes [13] and synergistic effects not necessarily related to spatial contacts [14–16].

Skwark *et al* applied a version of DCA to whole-genome sequencing data of a population of *Streptococcus pneumoniae* [17], and were able to retrieve interactions between members of the Penicillin-Binding Protein (PBP) family of proteins. Schubert *et al* performed a similar analysis on data from *Neisseria gonorrhoeae* [18]. Standard versions of DCA are rather compute-intensive for genome-scale inference tasks, but methodological speed-ups [19, 20] and alternative approaches [21] have been developed.

It is thus computationally feasible to infer interactions between widely separated loci from population-wide whole-genome data. The question then arises if the results obtained are also biologically meaningful *i.e.* if, and when, they reflect underlying identifiable mechanisms. In an earlier contribution [22], one of us argued that the reason should be sought in the *Quasi-Linkage Equilibrium* (QLE) of Kimura [23–25], as later extended by Neher and Shraiman to statistical genetics on the genome scale [26, 27]. In this paper we test this explanation by simulating an evolving population with known fitness parameters, treating the output of the simulation as data, and then using DCA and the Kimura-Neher-Shraiman theory (KNS) to infer fitness parameters.

We find that KNS indeed allows to infer fitness from data in broad, but not global, parameter ranges. Concerning the central parameter of KNS which is the overall rate of recombination, the theory works in an intermediate regime, while it fails at both a very high and very low rate. We discuss these limitations as well as performance when varying other parameters. We also discuss implications for inferring epistatic interactions from whole-genome population-wide data.

The paper is organized as follows. In Section II we summarize relevant results of the quasi-linkage equilibrium theory and in Section III we present the model and the simulation methods. In Section IV we show tests of inference procedure (7). Section V synthesizes such tests to phase diagrams of when fitness inference using (7) is possible/not possible in these models, while Section VI summarizes and discusses the results. Supplementary technical details are given in three appendices. In Appendix A we give parameter settings for simulations using the FFPopSim software introduced in Section III, and in Appendices B and C we give details on the nMF and PLM inference procedures which we have used.

## II. A QUASI-LINKAGE EQUILIBRIUM PRIMER

The concept Quasi-Linkage Equilibrium (QLE) is built on the distinction between Linkage Equilibrium (LE) and its opposite, Linkage Disequilibrium (LD). For completeness we will first describe these concepts for the case of two loci  $A$  and  $B$  where there can be, respectively,  $n_A$  and  $n_B$  alleles. The configuration of one genome with respect to  $A$  and  $B$  is then  $(x_A, x_B)$  where  $x_A$  takes values in  $\{1, \dots, n_A\}$  and  $x_B$  takes values in  $\{1, \dots, n_B\}$ . The configuration of a population of  $N$  individuals is the set  $\left[(x_A^{(s)}, x_B^{(s)})\right]$  where  $s$  ranges from 1 to  $N$ . This set defines the empirical probability distribution with respect to  $A$  and  $B$  as

$$P_{AB}(x_A, x_B) = \frac{1}{N} \sum_{s=1}^N \mathbf{1}_{x_A^{(s)}, x_A} \mathbf{1}_{x_B^{(s)}, x_B}, \quad (1)$$

\* hlzeng@njupt.edu.cn

† eaurell@kth.se

where  $\mathbf{1}_{a,b}$  is the Kronecker delta. Similarly we can define  $P_A(x_A) = \frac{1}{N} \sum_{s=1}^N \mathbf{1}_{x_A^{(s)}, x_A}$ , and  $P_B(x_B)$ . The distribution of genomes in a population over loci  $A$  and  $B$  is said to be in *Linkage Equilibrium* (LE) if the alleles  $a_A$  and  $x_B$  are independent under the empirical distribution *i.e.* if  $P_{AB}(x_A, x_B) = P_A(x_A)P_B(x_B)$ . All other distributions are in *Linkage Disequilibrium* (LD).

Independence implies that co-variances vanish. That is, if  $\langle \dots \rangle$  means averaging with respect to  $P$ , then in LE

$$C_{AB}(a, b) = \langle \mathbf{1}_{a, x_A} \mathbf{1}_{b, x_B} \rangle - \langle \mathbf{1}_{a, x_A} \rangle \langle \mathbf{1}_{b, x_B} \rangle = 0 \quad (2)$$

The co-variance matrix  $C_{AB}(a, b)$  always satisfies  $\sum_a C_{AB}(a, b) = \sum_b C_{AB}(a, b) = 0$  and therefore has  $(n_A - 1)(n_B - 1)$  independent components. For pairs of biallelic loci ( $n_A = n_B = 2$ ) it is convenient to label the alleles by another set of variables  $s$  that take values in  $\pm 1$ . For this case  $\langle \mathbf{1}_{1, x_A} \rangle = \frac{1}{2}(1 + \chi_A)$  and  $\langle \mathbf{1}_{2, x_A} \rangle = \frac{1}{2}(1 - \chi_A)$  where  $\chi_A = \langle s_A \rangle$ . Similarly  $C_{AB}(1, 1) = -C_{AB}(1, 2) = -C_{AB}(2, 1) = C_{AB}(2, 2) = \frac{1}{4}\chi_{AB}$  where

$$\chi_{AB} = \langle s_A s_B \rangle - \langle s_A \rangle \langle s_B \rangle \quad (3)$$

is the co-variance between loci  $A$  and  $B$ . In LE all the coefficients  $\chi_{AB}$  are zero.

*Quasi-Linkage Equilibrium* is a subset of distributions in LD which are characterized by a distribution over genotypes of the form (for biallelic loci)

$$P(\mathbf{s}) = \frac{1}{Z} \exp \left( \sum_i h_i s_i + \sum_{i < j} J_{ij} s_i s_j \right) \quad (4)$$

where  $Z$  (partition function) is the normalization. Obviously (4) is the Ising model of equilibrium statistical mechanics, which like all maximum-entropy models is characterized by its set of sufficient statistics that are here the “magnetizations”  $\chi_i$  and “correlations”  $\chi_{ij}$ . When all  $\chi_{ij}$  (and all Ising parameters  $J_{ij}$ ) are small (4) is close to the set of independent distributions which characterize LE.

The fundamental insight of Motoo Kimura into this problem was that distributions of the type (4) appear naturally in population genetics models which include biological recombination (or sex) [23–25]. If individual genomes are assimilated to configurations of a particle system, a recombination event is akin to a collision. In a mechanism analogous to relaxation to the equilibrium distribution in Boltzmann’s equation, (4) then holds for a high enough rate of recombination. The parameters  $h_i$  and  $J_{ij}$  of the genotype distribution are hence in this theory *consequences* of a dynamical evolution law for the population which takes into account recombination, mutations, varying fitness and carrying capacity. The mechanisms have been detailed previously [22, 26, 27] and will be reviewed again below in Section III.

Fitness is in Kimura-Neher-Shraiman (KNS) theory a function of the genotype

$$F(\mathbf{s}) = \sum_i f_i s_i + \sum_{i < j} f_{ij} s_i s_j \quad (5)$$

where the linear coefficients  $f_i$  are referred to as *additive contributions to fitness* and the quadratic (pairwise) coefficients  $f_{ij}$  are *epistatic contributions to fitness*. The most important relation in KNS is

$$J_{ij} = \frac{f_{ij}}{rc_{ij}} \quad (6)$$

where  $J_{ij}$  are the parameters of the distribution in (4),  $f_{ij}$  are the model parameters in (5),  $r$  is an overall rate of recombination, and  $c_{ij}$  is the probability that alleles at loci  $i$  and  $j$  are inherited from different parents. When recombination is large this probability will be close to  $\frac{1}{2}$  for most pairs of loci. Hence (6) can be interpreted as a *inference formula of epistatic fitness from genomic data*:

$$f_{ij}^* = J_{ij}^* \cdot rc_{ij} \quad (7)$$

where  $*$  indicates inferred value,  $J_{ij}^*$  is determined from data, and the remaining parameter  $r$  is a proportionality.

Formula (6) is derived under the assumption that mutation is low enough. This is a potential confounder because if the mutation rate is strictly zero the most fit genotype will eventually take over in a finite population. When this has happened one has instead of (4) the much simpler result

$$P(\mathbf{s}) = \mathbf{1}_{\mathbf{s}, \hat{\mathbf{s}}} \quad (8)$$

where  $\hat{\mathbf{s}}$  is the most fit genotype. Since there is no variability in data drawn from (8) there is therefore no way to infer parameters  $J_{ij}^*$  from data, and formula (7) cannot be used.

### III. MODEL AND SIMULATION METHODOLOGY

We consider a population with a carrying capacity of  $N$  individuals, which indicates the average size of the population is  $N$ . Each individual characterized by a genome of length  $L$  ( $L$  distinct loci). For simplicity we assume as above biallelic loci, and encode the alleles as  $+1$  (major allele) and  $-1$  (minor allele). The genotype of an individual is then a string  $\mathbf{s} = (s_1, \dots, s_L)$  where each variable  $s_i$  takes values in  $\pm 1$ . An evolving population is described by a time-dependent normalized probability distribution  $P(\mathbf{s}, t)$ . This section describes the mechanisms by which these changes are assumed to occur [22, 26, 27], and how we simulate those changes on the population level using the FFPopSim software package [28].

*a. Mutations* are random changes of the  $s_i$ , assumed to occur independently at different loci and in different individuals. We further assume that they are characterized by one overall rate  $\mu$ , which is the probability that any one allele at any locus in any individual changes per unit time (per generation). They hence lead to a simple gain-loss master equation

$$\frac{dP}{dt} \big|_{mut} = \mu \sum_{i=1}^L P(F_i \mathbf{s}) - P(\mathbf{s}) \quad (9)$$

where  $F_i$  (flip operator on locus  $i$ ) acts on strings as

$$F_i(s_1, \dots, s_i, \dots, s_L) = (s_1, \dots, -s_i, \dots, s_L) \quad (10)$$

*b. Fitness* Fitness variations were introduced above in (5). The effect of fitness is that the higher the value  $F(\mathbf{s})$  for an individual, the higher is the number of expected offspring of this individual in the next generation. On the population level this gives

$$\frac{dP}{dt}|_{fit} = P(\mathbf{s}) (F(\mathbf{s}) - \langle F \rangle) \quad (11)$$

where the average fitness, with respect to the given distribution, is

$$\langle F \rangle = \sum_{\mathbf{s}} P(\mathbf{s}) F(\mathbf{s}) \quad (12)$$

The coefficients in (5) are hence *rates* in this model, with dimension inverse time.

We characterize the epistatic contributions to fitness as a model parameter by

$$\sigma(\mathbf{f}) = \sqrt{\frac{2}{L(L-1)} \sum_{i < j} f_{ij}^2} \quad (13)$$

where we have assumed that the average of the  $f_{ij}$  is zero.

We note that in [26, 27] fitness variability was characterized by the standard deviation of the fitness function  $F(\mathbf{s})$  with respect to  $P$ . Although this better reflects the fluctuations of fitness in a population it is a derived parameter (it depends on  $P$ ) and hence less convenient in numerical testing.

*c. Genetic drift* is the randomness from a finite number of individuals in the population, where some genotypes may propagate and multiply from one generation to the next, and others die out.

In our set-up genetic drift can be formulated together with fitness by first having every individual  $a$  give rise to a random number  $k_a$  of offspring (identical copies of themselves). These numbers  $k_a$  are Poisson distributed with rates  $e^{\Delta t F_a}$  where  $\Delta t$  is the (short) generation time and  $F_a$  is the fitness of individual  $a$ . The total number of individuals is then  $N' = \sum_{a=1}^N k_a$  which is brought back to  $N$  by either copying a further  $N - N'$  uniformly randomly chosen individuals in the new population, or by randomly eliminating  $N' - N$  individuals. Mutations can be incorporated in the same frame-work by first randomly flipping each allele in every individual with probability  $\mu \Delta t$ .

The interplay between mutations and genetic drift are encoded in Fisher-Wright models, and has been studied since the beginning of population genetics [29], and has been reviewed many times, *e.g.* in [30]. On the level of distributions genetic drift gives rise to diffusion terms (Kimura's diffusion approximation).

*d. Recombination* is a way for two individuals (parents) pool their genomes to give rise to an individual with a genome that is a combination of the parents. The model presented in [26, 27] applies to haploid yeast. In such organisms an individual is ordinarily described by

one genome sequence  $\mathbf{s}$  (haploid phase). At the time of mating each individual additionally makes a second copy of their genome ("mating body") so that they temporarily hold two identical copies of  $\mathbf{s}$  (diploid phase). In recombination two mating bodies merge to make one new individual which carries one genome sequence  $\mathbf{s}$  containing a mix of the genetic information from the parents. By this process the total number of individuals grows by the number of pairs that have mated which is balanced by randomly eliminating a fraction of the new population so that the total remains  $N$ .

As discussed in [22] the model in [26, 27] basically also applies to forms of bacterial recombination. In that case two individuals (two bacteria) with genotypes  $\mathbf{s}_1$  and  $\mathbf{s}_2$  recombine with a rate  $rQ(\mathbf{s}_1, \mathbf{s}_2)$  where  $r$  an overall factor and  $Q(\mathbf{s}_1, \mathbf{s}_2)$  a relative rate. The outcome of the recombination is two individuals (two bacteria)  $\mathbf{s}'_1$  and  $\mathbf{s}'_2$  which can be specified by the indicator variable  $\xi$ :

$$\mathbf{s}'_1 : s_i^{(1)'} = \xi_i s_i^{(1)} + (1 - \xi_i) s_i^{(2)} \quad (14)$$

$$\mathbf{s}'_2 : s_i^{(2)'} = (1 - \xi_i) s_i^{(1)} + \xi_i s_i^{(2)} \quad (15)$$

and this outcome of the recombination happens with probability  $C(\xi)$ . The total rate of the individual event producing  $\mathbf{s}'_1$  and  $\mathbf{s}'_2$  from  $\mathbf{s}_1$  and  $\mathbf{s}_2$  is hence  $rQ(\mathbf{s}_1, \mathbf{s}_2)C(\xi)$ , and the change of the distribution over genotypes due to recombination is

$$\frac{d}{dt}P(\mathbf{s})|_{rec} = r \sum_{\xi, \mathbf{s}'} C(\xi) [Q(\mathbf{s}_1, \mathbf{s}_2)P(\mathbf{s}_1)P(\mathbf{s}_2) - Q(\mathbf{s}, \mathbf{s}')P(\mathbf{s})P(\mathbf{s}')] \quad (16)$$

From a physical point of view this type of recombination is analogous to a collision process where two-genome distributions on the right hand side of (16) have been assumed to factorize.

A central quantity in the theory is the probability that in the offspring of two individuals that have recombined the alleles on two loci  $i$  and  $j$  have been inherited from different parents:

$$c_{ij} = \sum_{\xi} C(\xi) (\xi_i(1 - \xi_j) + (1 - \xi_i)\xi_j) \quad (17)$$

If there is an *even* number of recombination events between  $i$  and  $j$  then the alleles at these two loci are inherited from *the same* parent. If on the other hand there is an *odd* number of recombination events between  $i$  and  $j$  then the alleles at these two loci are inherited from *different* parents. Therefore we also have

$$c_{ij} = p(1; i, j) + p(3; i, j) + p(5; i, j) + \dots \quad (18)$$

where  $p(k; i, j)$  is the probability to have  $k$  recombination events between  $i$  and  $j$ . These probabilities will in general depend on  $i$  and  $j$  and the distribution  $C(\xi)$  in a nontrivial manner.

A simple assumption that can be evaluated easily is if recombination can happen anywhere on a genome between two neighboring loci with uniform probability  $\rho$ . The number of recombination events between  $i$  and  $j$  is

then binominally distributed and

$$c_{ij} = \frac{1}{2} \left( 1 - \left( 1 - 2\rho \right)^{|i-j|} \right) \approx \frac{1}{2} \left( 1 - e^{-2\rho|i-j|} \right) \quad (19)$$

where the second line holds if  $\rho|i-j|$  is order unity and  $|i-j|$  is large. For pairs of loci sufficiently far apart we have  $c_{ij} \approx \frac{1}{2}$ , and (19) is the approximation we will use in the simulation.

*e. Parameters* The three important parameters we chose to study are  $\mu$ ,  $\sigma$  and  $r$  representing mutations, selection and recombination respectively.

Naturally this choice is stylized (or simplified), as modifications and additions can be made to all three mechanisms. Mutation rates in real organisms can and will vary between loci, and will typically not be the same in both directions. Gaussian distributed fitness variance are well characterized by the standard deviation, but other model distributions would depend on more parameters, for an example see *e.g.* the “random power-law distribution” introduced in [20]. As discussed above recombination for closely enough spaced loci depends even in the simplest model on parameter  $\rho$ . More generally recombination can have the same overall rate, but still differ greatly in *e.g.* the lengths of genomic sub-sequences interchanged between two individuals and along the genomes (“recombination hotspots”).

*f. FFPopSim* For simulations we have used the FFPopSim software package [28] with settings as described in Appendix A. FFPopSim allows for different types of recombination, each of which is described by a set of parameters; these parameters are given in Appendix A.

*g. Mutations, carrying capacity and length of simulation* As discussed above around (8) in the absence of mutations the most fit genotype will eventually take over a finite population. When this has happened all variability is lost, and it is no longer possible to infer epistatic contributions to fitness.

When mutation rates are non-zero but small the distribution should most of the time also resemble (8), and only for long enough times will the population at some loci swift between the available alleles. Fig. 1a shows that for sufficiently low mutation rates the population this is indeed the case. For higher mutation rates (Fig. 1b) frequencies fluctuate faster between the extremes, and at sufficiently high mutation rates (Fig. 1c) frequencies for most of the time hover around the entropically dominant configurations, where approximately half are up and half are down.

The size of the carrying capacity  $N$ , the mutation rate  $\mu$  and the simulation time (generation)  $T$  hence exert a combined effect on the simulations which impacts on tests of KNS theory. When  $N$  is very large, as it is likely to always be in real data from bacterial or fungal populations, one will have sufficient variability to estimate ensemble locus-locus correlations from data from one time. In such a case  $T$  can be ignored.

At intermediate values of  $N$ , as one will typically have in a simulation, then at moderate mutation rates, Fig. 1a, there is not enough variability in the population to estimate locus-locus correlations from data at one time. It

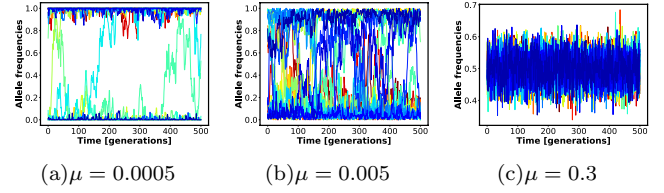


FIG. 1. Frequency of the first allele  $f_i[1]$  for all loci as function of time at different mutation rates  $\mu$ . Data output every five generations. This quantity is related to  $\chi_i$  defined in text by  $\chi_i = f_i[1] - 1$ . Population size  $N = 200$ , number of loci  $L = 25$ , recombination rate  $r = 0.05$ , crossover rate  $\rho = 0.5$  and fitness variability  $\sigma = 0.002$ . Pairwise epistatic fitness parameters  $f_{ij}$  are distributed as Gaussians (Sherrington-Kirkpatrick model), additive fitness parameters  $f_i$  are zero. The number of generations  $T = 5 \times 500$ . Panel (a): mutation rate  $\mu = 0.0005$ . For most loci the distribution is frozen to one value (0 or 1) for most of the simulation time; longer simulations would have been needed to gather enough data for inference. Panel (b): mutation rate  $\mu = 0.005$ . For many loci the distribution fluctuates away from the limiting value, although for most loci frequencies do not change over in the available simulation time. Panel (c): mutation rate  $\mu = 0.3$ . For all loci the frequencies change over multiple times.

is only if one uses data from different times that one can meaningfully test KNS theory in this range.  $T$  is hence here a meaningful parameter relative to  $N$  and  $\mu$ . For example, in Fig. 1b, there may be enough information in the time series to estimate correlations (and fitness) but in Fig. 1a there clearly cannot be since there is very little variation.

At high enough mutation rate, Fig. 1c there will again be enough variability to estimate correlations from data from one time, and  $T$  can again be ignored. However, the quantitative aspects of KNS theory such as inference formula (7) have been derived under the assumption that mutation is a weaker effect than recombination. Therefore in this range KNS cannot be expected to be quantitatively correct, whether applied to data from one time, or to data from a time series.

#### IV. INFERENCE METHODS AND THEIR PERFORMANCE IN DIFFERENT PHASES

The inverse Ising problem is to infer model parameters in the distribution (4) from data drawn independently from that same distribution. A large collective effort reviewed and summarized in [1] has led to a detailed understanding of when such a procedure can (or can't) work. The dimensions of the problem are

- number of samples ( $N$ )
- the average size and distribution of the underlying parameters ( $h$  and  $J$ )
- the inference procedure used

The main inference procedures in use are “naive” mean-field (nMF), pseudo-likelihood maximization (PLM) and Boltzmann machines. The latter is an iterative method

to find the maximum likelihood estimate of the parameters. In general performance and computational cost increases along this list. Boltzmann machines in particular are not feasible for large enough instances due to the exponential complexity of the computation of ensemble averages. We will therefore not consider that method further here.

As discussed above, snap-shot data at one time from a simulation of an evolving population at finite  $N$  is different from data drawn from an Ising/Potts distribution. Even if carrying capacity  $N$  is large enough to estimate correlations, these same correlations will fluctuate in time with amplitude  $N^{-\frac{1}{2}}$ , see [27] (Section VI and Appendix D). For these reasons we will use variants of nMF and PLM that use all the data in a simulation, a distinction which we underline by the qualifier *alltime*-.

nMF means to treat the model as Gaussian and is hence given by the matrix inversion formula

$$J_{ij}^* = -(\chi)^{-1}_{ij} \quad (20)$$

where  $\chi_{ij} = \langle s_i s_j \rangle - \chi_i \chi_j$ , and  $\chi_i = \langle s_i \rangle$  are correlations and means respectively.

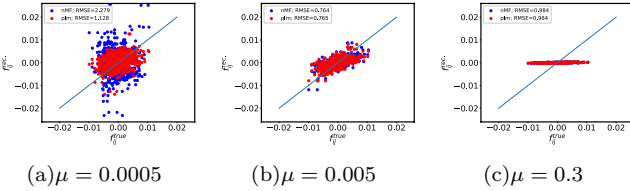


FIG. 2. Scatter-plots of inferred fitness parameters  $f_{ij}^*$  vs. model fitness parameters  $f_{ij}$ , all parameter values the same as in Fig. 1. Inference of Ising parameters  $J_{ij}^*$  is by the *alltime-nMF* and *alltime-PLM* procedures (described in main text). Inferred fitness parameters  $f_{ij}^*$  are determined from Ising parameters  $J_{ij}^*$  by the Kimura-Neher-Shraiman formula, (7). Panel (a): at low mutation rates the inferred fitness values are unrelated to the underlying model parameters (“a cloud of points”). Panel (b): at intermediate mutation rates there is sufficient variability in the data and the procedure is fairly accurate. Panel (c): at high mutation rates the inferred fitness values are everywhere small such that plot is an almost horizontal line.

*Alltime-nMF* means that we pool all the individuals from the whole population and all times into one large data set. From this we compute  $\chi_{ij}$  and  $\chi_i$ , and from there we infer the parameters  $J_{ij}^*$  using (20). Compared to nMF on data from one time, the computational cost of *alltime-nMF* scales linearly in  $T$  (time needed to compute the averages and correlation functions). Further details on *alltime-nMF* are given in Appendix B. We note that one can also consider the opposite approach of first using (20) on the data from each time, and then averaging the inferred  $J_{ij}^*$  over time. For parameter ranges where *alltime-nMF* works as an inference procedure we find that this second approach gives similar results (data not shown).

In contrast to nMF, PLM is a method to estimate parameters from conditional probabilities of one data item  $s_i$  (one spin) conditioned on all the others ( $\mathbf{s}_{\setminus i}$ ). For the

Ising model this conditional probability is

$$P(s_i | \mathbf{s}_{\setminus i}) = \frac{e^{h_i s_i + \sum_{j \neq i} J_{ij} s_i s_j}}{\sum_u e^{h_i u + \sum_{j \neq i} J_{ij} u s_j}}, \quad (21)$$

where  $u = \pm 1$  is the possible states of  $s_i$ . Compared to the full probability (4)  $P(s_i | \mathbf{s}_{\setminus i})$  only depends on a much smaller set of parameters, and is normalized in a way that is much simpler to deal with. Given a number of samples, assumed independent, one can then maximize the corresponding log-likelihood function

$$PL_i(h_i, \{J_{ij}\}) = h_i \langle s_i \rangle + \sum_{j \neq i} J_{ij} \langle s_i s_j \rangle - \left\langle \log \sum_u e^{h_i u + \sum_{j \neq i} J_{ij} u s_j} \right\rangle \quad (22)$$

Maximizing  $PL_i$  will give inferred parameter “as seen from  $i$ ”, symbolically written  $h_i^*$  and  $J_{ij}^*$ . Since in fact there is only one Ising model parameter  $J_{ij}$ , PLM must be complemented by an output procedure for which a standard choice is

$$J_{ij}^* = \frac{1}{2} (J_{ij}^{*i} + J_{ij}^{*j}) \quad (23)$$

*Alltime-PLM* means that we consider the whole population at all times in the simulation as  $N \cdot T$  samples from the same probability distribution, and use those to compute the log-likelihood functions  $PL_i$  in (22). The computational cost of *alltime-PLM* is considerably heavier than *alltime-nMF* essentially because there are many terms in the pseudo-log partition function, the last term in (22). In Appendix C we give further details on *alltime-PLM*, including estimates of computation times.

Using the same parameters and data as in Fig. 1, one then finds that inference of fitness is not possible at low mutation rates: the scatter-plot in Fig. 2a is but a cloud of points with no visible trend. At intermediate mutation rates Fig. 2b inference by KNS (7) works, while for large mutation rates Fig. 2c (7) does not work again.

## V. PHASE DIAGRAMS

Large-scale tests of inference as in Fig. 2 requires a quantitative criterion for when inference is successful or not. Here we will use the *normalized  $L_2$  distance* given by

$$\epsilon = \sqrt{\frac{\sum_{i < j} (f_{ij}^* - f_{ij})^2}{\sum_{i < j} f_{ij}^2}}. \quad (24)$$

When  $\epsilon$  is much smaller than one then inference is successful and the scatter-plots will look more or less like Fig. 2b (or better). On the other hand  $\epsilon$  can take values of around one or larger, either because  $f_{ij}^*$  and  $f_{ij}$  are about the same size but uncorrelated, as in Fig. 2a, or if  $f_{ij}^*$  appears as a function of  $f_{ij}$  but of another form. This is so in Fig. 2c where  $f_{ij}^*$  is close to zero for all pairs of loci, but other dependencies yielding similar  $\epsilon$  could also

be present.

We can now display the phase diagram by plotting  $\epsilon$  in (24) as function of parameters, color coded by the value of  $\epsilon$ . Fig. 3 shows this for the two inference formulas in the plane of mutation rate  $\mu$  versus recombination rate  $r$ . With (7) we qualitatively expect that inference will not work for sufficiently low recombination, because then this assumptions behind this formula are not satisfied (as will be shown below in Fig. 4a) and also not for very high recombination while low mutation neither, as will be illustrated in Fig. 4c. Essentially this turns out to be correct. In Fig. 3 fitness variations are everywhere small compared to mutations and recombination.

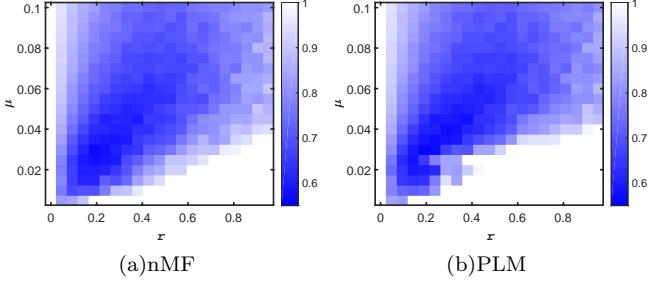


FIG. 3. Phase diagram of epistatic fitness inference quality color coded by the reconstruction error  $\epsilon$  in (24). Panel (a): fitness estimated by formula (7) with *alltime-nMF* procedure. Panel (b): fitness estimated by formula (7) with *alltime-PLM* procedure. By the color coding both schemes work in a very broad range of parameters. For large recombination inference does not work for the reasons illustrated in Fig. 4c, while for small recombination the assumptions underlying (7) are not satisfied, as shown in Fig. 4a.

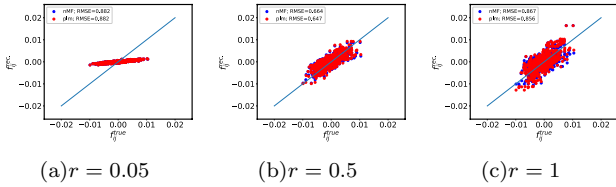


FIG. 4. Examples of inference results for different recombination rates  $r$  corresponding to three horizontally separated points in the middle of Fig. 3. Mutation rate  $\mu = 0.05$ , cross over rate  $\rho = 0.5$ , fitness variation  $\sigma = 0.002$ . Using parameters  $J_{ij}^*$  inferred by the *alltime-nMF* and *alltime-PLM* procedures, fitness values inferred from (7). Panel (a)  $r = 0.05$  shows that (7) underestimates fitness, through there appears to be a functional relation. Panel (b)  $r = 0.5$  shows that both procedures estimate the fitness fairly accurately. Panel (c)  $r = 1.0$  shows KNS works worse compared with that for mediate  $r$  presented in Panel (b).

Fig. 5 similarly shows  $\epsilon$  in the plane of fitness variations vs. recombination rate. Also here inference works using formula (7) at intermediate values of mutation rate  $\mu = 0.05$ . Qualitatively this corresponds to the setting of Fig. 2b where  $\epsilon$  is less than one. For small recombination and large recombination we would not expect inference to work for the reasons as discussed above. Additionally, in the simulations reported in Fig. 5, apparently the fitness variability was not high enough for the last effect to

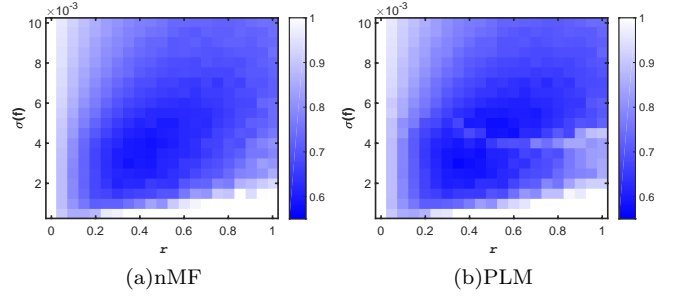


FIG. 5. Phase diagram of epistatic fitness inference with parameters fitness  $\sigma$  and recombination  $r$ . The mutation rate  $\mu = 0.05$ , cross over rate  $\rho = 0.5$ . The inference procedures are the same with that for Fig. 3. By the color coding two schemes work in a very broad range of parameters. For large recombination and very small variations inference does not work.

show up. This is confirmed by Fig. 6, which shows the inference works worse with increasing fitness variations.

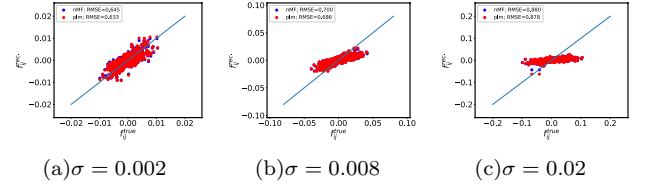


FIG. 6. Examples of inference results for different fitness variations  $\sigma$  with recombination rate  $r = 0.5$  corresponding to three vertically separated points through the middle of Fig. 5. Mutation rate  $\mu = 0.05$ , cross over rate  $\rho = 0.5$ . Panel (a):  $\sigma = 0.002$  shows both procedures estimate the fitness correctly. Panel (b):  $\sigma = 0.008$  shows that (7) underestimates fitness, through there appears to be a functional relation with less scatter than in Panel (a). Panel (c):  $\sigma = 0.02$  (beyond the vertical range of Fig. 5) shows that inference from (7) is approximately flat *i.e.* uninformative.

## VI. DISCUSSION

In this paper we have presented numerical evidence that pair-wise fitness parameters in an evolving population can be recovered from a distribution over genotypes. Conceptually this allows to integrate the Direct Coupling Analysis (DCA) technique [4–6] into the classic framework of population genetics [29, 30]. We hope this will lead to further studies into when and how such a connection can be made, and how to make it more precise.

An important conclusion of this work is that while recovery is possible in broad parameter ranges it is not universally so. In this sense the basis for DCA proposed here is quite different from max-entropy arguments. For this reason we summarize the main regions where recovery is *not* possible.

First, recovery is not possible for large recombination rate and small fitness variations. This is so because in this range the  $J_{ij}$  parameters which are inferred by DCA



are small and subject to small-sample noise. This limitation is analogous to the limitations on DCA when applied to finite data drawn from an Ising/Potts distribution, and which have been investigated in the past by many groups [1].

Second, for a given population size ( $N$ ) and given simulation/observation time ( $T$ ) recovery is not possible if mutation rate ( $\mu$ ) is low enough. This is so because for such populations the structure is essentially frozen. The underlying equations contain well-defined epistatic effects but those are not reflected in the population structure over the time  $T$ , and hence cannot be recovered from population data. Although of different origin this is similar to the limitations on DCA when applied to data drawn from the Sherrington-Kirkpatrick model in the low-temperature (spin-glass) phase, well investigated in the literature [1]. In that latter case thermalization is slow and many Monte Carlo updates are needed before two samples become uncorrelated; the simulation/observation time ( $T$ ) plays a similar role in our setting.

Third, recovery is not possible when mutation rate is comparable to or larger than recombination rate. In the data presented in this paper this is exemplified by Figs. 2c, 4a, 6b and 6c. This discrepancy has no analogue in inverse Ising studies, and is instead, we believe, because in these parameter ranges the Quasi-Linkage Equilibrium theory of Kimura, Neher and Shraiman [23–27] is not applicable. In contrast to when recombination dominates over mutations there is no argument known to us for what the population structure should then be. It could be something very different from a Ising/Potts distribution, but it could also be an Ising/Potts distribution with other relations among the parameters. We note that especially Fig 6b appears to point a relation between fitness and the  $J_{ij}$ 's, but which is not well captured QLE inference formula of (7). In any case, to understand the connection between epistatic fitness ( $f_{ij}$ ) and population structure ( $J_{ij}$ ), if any, is an important and unsolved problem. We hope to be able to return to this problem in a future contribution.

Finally, we note that the whole analysis in this paper is based on the concept of fitness landscapes. Fitness is thus here an inherent (and heritable) property of each individual reflected in its expected number of offspring, and one can imagine such fitness to be optimized. While in this class of models absolute fitness depends on the whole population structure, the relative order of fitness of two individuals does not. Darwinian fitness and natural selection is in contrast a wider concept including also competition and cooperation. The relation between fitness and population structure when such aspects of strategy and game theory are dominant are clearly very interesting, but lie beyond the range of approaches considered here.

## ACKNOWLEDGMENTS

We thank Simona Cocco, Eugenio Mauro, Rémi Monasson and Guilhem Semerjian for discussions and Richard Neher for the FFPopSim software package

and comments. The work of HLZ was supported by National Natural Science Foundation of China (11705097), Natural Science Foundation of Jiangsu Province (BK20170895), Natural Science Foundation for Colleges and Universities in Jiangsu Province (17KJB140015) Jiangsu Government Scholarship for Overseas Studies of 2018, and Scientific Research Foundation of Nanjing University of Posts and Telecommunications (NY217013). The work of EA was partially supported by Foundation for Polish Science through TEAM-NET project (contract no. POIR.04.04.00-00-17C1/18-00).

## Appendix A: FFPopSim settings

The FFPopSim package was written by Fabio Zanini and Richard Neher and simulates an evolving population with biallelic loci and additive as well as pairwise epistatic fitness functions [28]. We here describe first default parameters which have the same values in all simulations reported in this paper, and then how we have varied simulation parameters to obtain the different figures.

### 1. FFPopSim default parameters

The default parameters of FFPopSim we used in the simulations are listed in Tab. I. The value of them is the same for the results presented here.

TABLE I. Main default parameters of FFPopSim used in the simulation.

number of loci (L)	25
circular	True
carrying capacity (N)	200
generation	$500 \times 5$
recombination model	CROSSOVERS
crossover rate ( $\rho$ )	0.5
fitness additive(coefficients)	0.0
number of traits	1

### 2. FFPopSim parameter varied

The following parameters in FFPopSim are varied in the presented inference for epistatic fitness

TABLE II. Varied parameters of FFPopSim used in the simulation.

outcrossing rate ( $r$ )	$[0., 1.0]$
mutation rate ( $\mu$ )	$[0.005, 0.1]$
fitness coefficients	Gaussian random
	number with std. $\sigma \in [0.0005, 0.01]$
initial genotypes	binary random numbers

## Appendix B: Naive mean-field use (nMF)

The multi-locus evolution is done by the “evolve()” function for each generation with FFPopSim. The correlations  $\chi_{ij}$ s are computed and recorded for each generation. When the “evolve” process is done, the mean correlations  $\langle\chi_{ij}\rangle$  over generations are computed and used for the inference. The pseudo-code for nMF inference is presented in Algorithm 1.

---

### Algorithm 1: Epistatic fitness inference by nMF

procedure:  $f_{ij}^{nMF}$

---

**Input:** mean correlations:  $\langle\chi_{ij}\rangle$

**Output:** inferred epistatic fitness:  $f_{ij}^{nMF}$

```

1: import scipy
2: from scipy import linalg
3:  $J_{ij}^{nMF} = -\text{linalg.inv}(\langle\chi_{ij}\rangle)$ 
4:  $f_{ij}^{nMF} = J_{ij}^{nMF} * r * c_{ij}$ 

```

---

## Appendix C: Pseudo-likelihood maximization use (PLM)

Ising model parameters are inferred by the Pseudo-likelihood maximization method [31] using the matlab software PLM at [32] ([www.github.com/gaochenyi/CC-PLM](http://www.github.com/gaochenyi/CC-PLM)). The allele states are recorded for each generation. A giant matrix with an approximate size of  $25 \times N \times T$  produced by FFPopSim is the input of PLM software for the Ising parameters  $J_{ij}^{PLM}$ . The pseudo-code for PLM inference is Algorithm 2.

With  $L = 25$  loci and the rest of parameters are the same, the CPU-time for  $N = 200$  and  $T = 500$  on a standard desktop computer is about 50 seconds and it is dominated by the PLM process. It increases linearly with increasing  $N$  or  $T$ . For instance, it will be around 3000 seconds for  $N = 2000$  and  $T = 2000$ , in which the PLM process costs about 2300 seconds.

---

### Algorithm 2: Epistatic fitness inference by PLM

procedure:  $f_{ij}^{PLM}$

---

**Input:** Giant binary state matrix **S** with an

approximate size of  $L \times N \times T$

**Output:** inferred epistatic fitness:  $f_{ij}^{PLM}$

```

1: import matlab.engine
2: eng = matlab.engine.start_matlab()
3:  $J_{ij}^{PLM} = \text{eng.plm\_to\_ffpopsim}(\mathbf{S})$ 
4:  $f_{ij}^{PLM} = J_{ij}^{PLM} * r * c_{ij}$ 

```

---

- 
- [1] H. C. Nguyen, R. Zecchina, and J. Berg, *Adv. Phys.* **66**, 197 (2017).
  - [2] M. Weigt, R. A. White, H. Szurmant, J. A. Hoch, and T. Hwa, *Proc. Natl. Acad. Sci.* **106**, 67 (2009).
  - [3] F. Morcos, A. Pagnani, B. Lunt, A. Bertolino, D. S. Marks, C. Sander, R. Zecchina, J. N. Onuchic, T. Hwa, and M. Weigt, *Proc. Natl. Acad. Sci.* **108**, E1293 (2011).
  - [4] R. R. Stein, D. S. Marks, and C. Sander, *PLoS Comput. Biol.* **11**, e1004182 (2015).
  - [5] M. Michel, M. J. Skwark, D. Menéndez Hurtado, M. Ekeberg, and A. Elofsson, *Bioinformatics* **33**, 2859 (2017).
  - [6] S. Cocco, C. Feinauer, M. Figliuzzi, R. Monasson, and M. Weigt, *Rep. Prog. Phys.* **81**, 032601 (2018).
  - [7] S. Ovchinnikov, H. Park, N. Varghese, P.-S. Huang, G. A. Pavlopoulos, D. E. Kim, H. Kamisetty, N. C. Kyrpides, and D. Baker, *Science* **355**, 294 (2017).
  - [8] M. Michel, D. Menéndez Hurtado, K. Uziela, and A. Elofsson, *Bioinformatics* **33**, i23 (2017).
  - [9] S. Ovchinnikov, H. Park, D. E. Kim, F. DiMaio, and D. Baker, *Proteins* **86**, 113 (2018).
  - [10] E. De Leonardis, B. Lutz, S. Ratz, C. Simona, R. Monasson, M. Weigt, and A. Schug, *Nucleic Acids Res.* **43**, 10444 (2015).
  - [11] T. Gueudré, C. Baldassi, M. Zamparo, M. Weigt, and A. Pagnani, *Proc. Natl. Acad. Sci.* **113**, 12186 (2016).
  - [12] G. Uguzzoni, S. John Lovis, F. Oteri, A. Schug, H. Szurmant, and M. Weigt, *Proc. Natl. Acad. Sci.* **114**, E2662 (2017).
  - [13] C. Weinreb, A. J. Riesselman, J. B. Ingraham, T. Gross, C. Sander, and D. S. Marks, *Cell* **165**, 963 (2016).
  - [14] M. Figliuzzi, H. Jacquier, A. Schug, O. Tenaillon, and M. Weigt, *Mol. Biol. Evol.* **33**, 268 (2016).
  - [15] T. A. Hopf, J. B. Ingraham, F. J. Poelwijk, C. P. I. Scharfe, M. Springer, C. Sander, and D. S. Marks, *Nat. Biotechnol.* **35**, 128 (2017).
  - [16] A. Couce, L. V. Caudwell, C. Feinauer, T. Hindré, J.-P. Feugeas, M. Weigt, R. E. Lenski, D. Schneider, and O. Tenaillon, *Proc. Natl. Acad. Sci.* **114**, E9026 (2017).
  - [17] M. J. Skwark, N. J. Croucher, S. Puranen, C. Chewapreecha, M. Pesonen, Y. Y. Xu, P. Turner, S. R. Harris, S. B. Beres, J. M. Musser, J. Parkhill, S. D. Bentley, E. Aurell, and J. Corander, *PLoS Genet.* **13**, e1006508 (2017).
  - [18] B. Schubert, R. Maddamsetti, J. Nyman, M. R. Farhat, and D. S. Marks, *Nat. Microbiol.* **4**, 328 (2019).
  - [19] S. Puranen, M. Pesonen, J. Pensar, Y. Y. Xu, J. A. Lees, S. D. Bentley, N. J. Croucher, and J. Corander, *Microb. Genom.* (2018).
  - [20] C.-Y. Gao, H.-J. Zhou, and E. Aurell, *Phys. Rev. E* **98**, 032407 (2018).
  - [21] J. Pensar, S. Puranen, B. Arnold, N. MacAlasdair, J. Kuronen, G. Tonkin-Hill, M. Pesonen, Y. Xu, A. Sipola, L. Sánchez-Busó, J. A. Lees, C. Chewapreecha, S. D. Bentley, S. R. Harris, J. Parkhill, N. J. Croucher, and J. Corander, *Nucleic Acids Res.* **47**, e112 (2019).



- [22] C.-Y. Gao, F. Cecconi, A. Vulpiani, H.-J. Zhou, and E. Aurell, *Phys. Biol.* **16**, 026002 (2019).
- [23] M. Kimura, *Evolution* **10**, 278 (1956).
- [24] M. Kimura, *J. Appl. Probab.* **1**, 177–232 (1964).
- [25] M. Kimura, *Genetics* **52**, 875 (1965).
- [26] R. A. Neher and B. I. Shraiman, *Proc. Natl. Acad. Sci.* **106**, 6866 (2009).
- [27] R. A. Neher and B. I. Shraiman, *Rev. Mod. Phys.* **83**, 1283 (2011).
- [28] R. Neher and F. Zanini, “Ffpopsim,” <http://code.google.com/p/ffpopsim/> (2012).
- [29] R. Fisher, *The Genetical Theory of Natural Selection* (Clarendon, 1930).
- [30] R. A. Blythe and A. J. McKane, *J. Stat. Mech.: Theory Exp.* **2007**, P07018 (2007).
- [31] M. Ekeberg, T. Hartonen, and E. Aurell, *J. Comput. Phys.* **276**, 341 (2014).
- [32] C.-Y. Gao, “gaochenyi/cc-plm,” Github (2018).